THE JOURNAL OF PHYSICAL CHEMISTRY B

Article

pubs.acs.org/JPCB

Impact of Hydrogen Bonding on the Dynamics and Structure of Protic Ionic Liquid/Water Binary Mixtures

Heather E. Bailey, Yong-Lei Wang, and Michael D. Fayer*

Department of Chemistry, Stanford University, Stanford, California 94305, United States

ABSTRACT: The orientational dynamics and microscopic liquid structure of a protic ionic liquid, 1-ethylimidazolium bis(trifluoromethylsulfonyl)imide (EhimNTf$_2$), and its aprotic analogue, 1-ethyl-3-methylimidazolium bis(trifluoromethylsulfonyl)imide (EmimNTf$_2$), were studied at various water concentrations using optical heterodyne-detected optical Kerr effect (OHD-OKE) spectroscopy, linear infrared spectroscopy, and atomistic simulations. The OHD-OKE experiments essentially measure the orientational relaxation of the Ehim$^+$ and Emim$^+$ cations. The experiments and simulations show a significant dynamical and structural change in EhimNTf$_2$ between the 2:1 ion pair:water and the 1:1 ion pair:water concentrations. The OHD-OKE data show that EmimNTf$_2$/water mixtures exhibit hydrodynamic behavior at all water concentrations up to saturation. In contrast, EhimNTf$_2$/water mixtures deviate from hydrodynamic behavior at water concentrations above 2:1. At the 1:1 concentration, the orientational randomization of the Ehim$^+$ cation is slower than that predicted using viscosity data. Atomistic simulation results reveal the microscopic ionic structures of dry liquids and the preferential hydrogen bonding of water to the H atom of the N−H of Ehim$^+$ over other sites on the Ehim$^+$ and Emim$^+$ cations. Atomistic simulation results demonstrate that in EhimNTf$_2$ RTIL/water mixtures there is a substantial jump in the formation of water−water hydrogen bonds in addition to N−H-water hydrogen bonds upon increasing the water concentration from 2:1 to 1:1. Water−water hydrogen bonding strengthens the spatial coordination of the H atom of the N−H moiety of Ehim$^+$ to neighboring water molecules through preferential hydrogen bonding. The jump in the concentration of water−water hydrogen bonds occurs at the Ehim$^+$/water concentration at which the orientational relaxation deviates from hydrodynamic behavior. This structural observation is confirmed with FT-IR spectra that show asymmetry in the peak for the O−D stretch that is indicative of water clusters. The formation of water clusters and the strengthening of the N−H···OH$_2$ hydrogen bonds slow the orientational relaxation of Ehim$^+$ cations as observed by the OHD-OKE experiments.

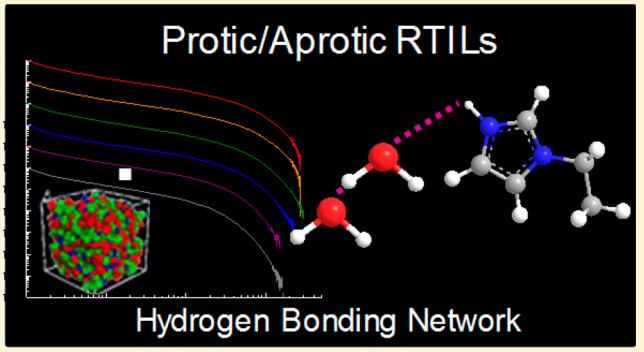

INTRODUCTION

Room temperature ionic liquids (RTILs) are charged species with melting points below 25 °C. Recently, RTILs have been widely studied due to their many unique and advantageous properties, such as low vapor pressure, nonvolatility, nonflammability, and thermal stability. These properties have made RTILs useful for many applications ranging from electrochemistry to synthesis. Ionic liquids are usually composed of an inorganic anion and an organic cation that have symmetry, size, or charge delocalization which frustrates the crystallization of the compound.[1,2] There are a vast number of cation and anion combinations that form ionic liquids with different physicochemical properties. The large number of available ions allows many properties of the RTIL, including viscosity and reactivity, to be optimized for best performance in an application.

One subclass of RTILs that has been of recent interest is protic ionic liquids (PILs). PILs are formed through the reaction of a Brønsted-Lowry acid and a Brønsted-Lowry base resulting in a cation with a readily available proton.[3,4] This proton enables the cation to have significant hydrogen bonding interactions in addition to the Coulombic interactions and dispersion forces that aprotic ionic liquids (AILs) have. The addition of hydrogen bonding to the intermolecular interactions affects many properties including melting points, viscosities, and water solubility.[5] PILs are often capable of stronger interactions with water than AILs because they can become part of water's hydrogen bonding network. PILs can generally take up more water than structurally similar AILs.

Research on PILs has increased due to their utility in electrochemistry,[3,6,7] biochemistry,[8] and inorganic and organic synthesis.[4] They have also shown promise in increasing the role of RTILs in carbon capture since ionic liquids with hydrogen bonds have been shown to dissolve more CO_2 than other ionic liquids.[9,10] Additionally, PILs are less expensive and often of higher purity due to the relative simplicity of their synthesis. Perhaps, the most significant applications of PILs are in energy conversion devices like batteries and fuel cells. Ionic liquids, particularly low viscosity RTILs like those containing bis(trifluoromethylsulfonyl)imide (NTf_2^-) anions,[11] are useful in batteries because they are nonflammable unlike traditional

Received: June 28, 2017
Revised: August 12, 2017
Published: August 15, 2017

DOI: 10.1021/acs.jpcb.7b06376
J. Phys. Chem. B XXXX, XXX, XXX−XXX

organic solvents. However, PILs have additional benefits including increasing the mobility of dissolved lithium ions.[12] PILs are also useful in fuel cells due to their ability to provide protons without requiring water as a proton source.[13]

In practical applications, ionic liquids are rarely neat since they are generally hygroscopic and readily pick up water from the environment. To avoid this, RTILs must be desiccated and kept in a dry environment, which may be time and cost prohibitive in many applications, particularly on an industrial scale. Therefore, it is useful to study the effect of water on the physicochemical and structural properties of ionic liquids. It has been demonstrated that many properties like viscosity,[14,15] diffusion coefficients,[16] and surface tension[17] are very sensitive to water concentration. In electrochemical applications like batteries and fuel cells, the conductivity[7] and its water dependence are important considerations. As water is added, there are two competing factors influencing conductivity. First, the viscosity generally decreases as the water concentration increases which allows greater charge mobility. However, water also dilutes the charge carriers. Thus, these two factors play off each other such that water increases conductivity up to a point.[18] Understanding more about how water influences the properties of ionic liquids can help optimize water as a solute in RTILs. This work aims to address the dynamics and liquid structures of RTIL/water mixtures, with particular focus on PILs.

RTIL/water mixtures have been studied using many methods including nuclear magnetic resonance,[19−21] optical Kerr effect spectroscopy,[22,23] and theoretical calculations.[24−27] PILs have been studied using a variety of techniques including ultrafast methods,[28,29] dielectric spectroscopy,[30] neutron scattering,[31] and molecular dynamics calculations.[21,32−34] Despite the wide range of research, there has not been a study of the bulk dynamics of PILs and the relationship of the dynamical properties to microstructures. Bulk dynamics can give insight into how PILs behave differently than AILs. Here we present results that increase understanding of the relationship between PILs and AILs and the influence of water by using optical heterodyne-detected optical Kerr effect spectroscopy (OHD-OKE) to study bulk dynamics from the subpicosecond range to the end of the orientational randomization many decades of time later. OHD-OKE is a unique ultrafast method because it allows dynamics to be tracked without the introduction of a solute to serve as a probe, so it truly tracks pure bulk dynamics. Linear infrared spectroscopy is used to provide an experimental observable related to the structural features that contribute to the dynamics observed in the OHD-OKE experiments. Atomistic simulations are performed to complement the experiments by providing microscopic details of the liquid structures in AILs and PILs at varied water contents.

EXPERIMENTAL PROCEDURES

Sample Preparation. Figure 1 gives the structures of 1-ethyl-3-methylimidazolium bis(trifluoromethylsulfonyl)imide ($EmimNTf_2$) (R = CH_3) and 1-ethylimidazolium bis(trifluoromethylsulfonyl)imide ($EhimNTf_2$) (R = H). The ring adjacent hydrogens and carbons are labeled in red on this structure. These labels will be used during the discussions. $EmimNTf_2$ is a well-studied ionic liquid due to its chemical stability and low viscosity, which makes it an ideal solvent in many applications.[11] The short alkyl chain of the imidazolium ring (having an ethyl group instead of a longer chain) eliminates extensive apolar regions in the liquid as shown in

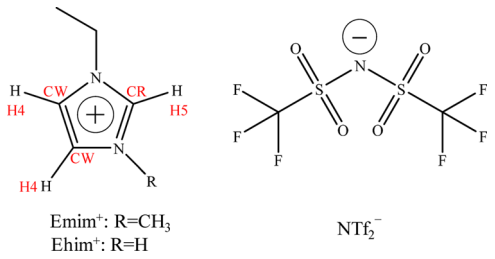

Figure 1. Chemical structures of 1-ethyl-3-methylimidazolium bis(trifluoromethylsulfonyl)imide ($EmimNTf_2$) (R = CH_3) and 1-ethylimidazolium bis(trifluoromethylsulfonyl)imide ($EhimNTf_2$) (R = H). In the imidazolium ring, the carbon atom between two nitrogen atoms is named as CR, and the other two carbon atoms in the same ring are labeled as CW. The corresponding directly bonded hydrogen atoms are designated as H5 and H4, respectively. These notations will be used in the discussions.

previous atomistic simulations.[35] $EhimNTf_2$ is identical to $EmimNTf_2$ except that the methyl group attached to the imidazolium is replaced by a hydrogen atom. This choice of liquids permits a direct comparison between a protic and an aprotic cation. In addition to studying the dry liquids, we compare both ionic liquids at multiple water concentrations up to their saturation points. Water does not contribute significantly to OHD-OKE signal because it does not have substantial anisotropic polarizability. In addition, detailed calculations demonstrate that the signal, which depends on the polarizability anisotropy, arises almost exclusively from the cations.[36] Therefore, the experiments are observing the orientational relaxation of $Emim^+$ and $Ehim^+$ cations.

$EmimNTf_2$ (99%) and $EhimNTf_2$ (97%) were purchased from Iolitec. Both ionic liquids were dried under vacuum to remove residual water. The water content of the dried samples was measured as 5 ppm for $EmimNTF_2$ and 24 ppm for $EhimNTf_2$ by coulometric Karl Fischer titration (Mettler Toledo). It has been shown that water contents less than 100 ppm have a negligible effect on the viscosity of $EmimNTf_2$.[14] Samples were prepared by mass at five and seven water concentrations ranging from dry to saturated solutions for $EmimNTf_2$ and $EhimNTf_2$, respectively. Water saturation was determined by adding excess water and mixing such that an emulsion formed. The mixture was allowed to sit over 24 h until two distinct layers formed. The water content of the water saturated ionic liquid was measured as 2.6 ion pairs per water for $EmimNTf_2$ and 0.65 ion pairs per water for $EhimNTf_2$, using Karl Fischer titration. All samples were filtered using a 0.02 μm filter (Whatman Anotop) into 1 cm path length optical grade cuvettes for use in the OHD-OKE experiments. The viscosity of each sample was measured using Cannon-Ubbelohde viscometry and pycnometry at the OHD-OKE experimental temperature of 24.4 °C.

$EhimNTf_2$ was deuterated (the H atom of the N−H moiety of the $Ehim^+$ cation was replaced by a D atom) to investigate the chemical environment of the N-D stretch via FT-IR. $EhimNTf_2$ was mixed overnight with CH_3OD (Sigma, 99% D) in a 1:100 mol ratio. Methanol was evaporated under vacuum for 3 days until only the deuterated ionic liquid ($Ehim\text{-}DNTf_2$) remained. The N−H is much more acidic than the other hydrogen atoms that are bonded to the imidazolium ring in $Ehim^+$, so it was selectively deuterated. FT-IR data were collected using CaF_2 windows and a 150 μm sample path length on a solution of 5% $Ehim\text{-}DNTf_2$ in $EhimNTf_2$. For

DOI: 10.1021/acs.jpcb.7b06376
J. Phys. Chem. B XXXX, XXX, XXX−XXX

solutions with water, a 5% HOD in H_2O solution was added to maintain the same amount of deuteration. FT-IR spectra for nondeuterated $EhimNTf_2$ were subtracted from the deuterated samples at the same water concentration. This resulted in spectra of only vibrations related to the N-D group in the $Ehim\text{-}D^+$ cation and the O−D group in HOD.

Optical Heterodyne-Detected Optical Kerr Effect Spectroscopy. The OHD-OKE setup has been described thoroughly previously.[22,23] A brief summary follows. Pulses are generated by an 86 MHz Ti:sapphire oscillator and then amplified by a 5.4 kHz Ti:sapphire regenerative amplifier. The amplified pulses are beam split into the pump and probe pulses. The pump beam proceeds directly to the sample and arrives linearly polarized. The probe beam arrives at the sample polarized at 45° relative to the pump after passing down a mechanical delay line. This delay allows data to be collected at many time points to measure the complete decay. Heterodyne detection is introduced into OHD-OKE experiments by making the probe pulse slightly elliptical just prior to the sample. This creates a collinear local oscillator that amplifies the signal and enables phase cycling for reduction of noise.[37,38]

The OHD-OKE experiment is a nonresonant pump−probe method that tracks the bulk motion of molecules via the time-dependent birefringence induced in the sample by an optical pulse. It provides the unique ability to track the orientational relaxation of molecules from the subpicosecond range to the end of orientational randomization many decades later. The OHD-OKE method measures the time derivative of the polarizability-polarizability (orientational) correlation function after very early time when collision-induced perturbations lead to brief multiparticle contributions to the signal. Extracting quantitative information (the correlation function) from the data can be difficult. The correlation function can be modeled by solving the set of differential equations that couple the orientational and density correlation functions with schematic mode coupling theory (MCT).[39] While the MCT solutions fit the data well and give shapes and time scales of the two correlation functions, they fail to provide easily comparable functions for the randomization processes on different time scales that can be readily compared for different samples. The general nature of the decays are several power laws that reflect the short time cage relaxation of molecules followed by a final exponential time decay that is associated with the global final randomization as the molecules return to their original isotropic orientation.[40] This final exponential can be related to many physical properties including the viscosity. Here the data displays the longest time scale power law, the von Schweidler power law,[40] followed by the long time scale exponential decay.

To obtain the correct exponential time constant and to improve determination of the power law exponents compared to a previous approach using a simple fitting function,[22,23,41−44] a new functional form, given in eq 1, was used.

$$F(t) = \frac{B}{2}\left(1 - \mathrm{erf}\left(\frac{(\ln(t) - n)}{\sqrt{2}\,u}\right)\right)t^{-b} + \frac{C}{2}\left(1 + \mathrm{erf}\left(\frac{\ln(t) - n}{\sqrt{2}\,u}\right)\right)e^{-t/\tau} + y_0 \quad (1)$$

The error functions are used to essentially turn off and turn on each function such that its influence does not bleed into time scales of other relaxation processes in the curve fitting. This is consistent with the basic physics of the processes in which each process, reflected by a different functional form in the decay, gives way to the next process rather than all functional forms existing over all times. The previous method can lead to small errors in some circumstances.[22,23,41−44] However, all trends previously reported should be the same. Eq 1 is shown for a single power law and an exponential, but the equivalent form is used if it is necessary to include more power laws in the data analysis. The parameters n and u determine the midpoint and width of the crossover region between the power law caging process and the exponential randomization process. B and b describe the amplitude and exponent of the von Schweidler power law. The final exponential describes a Markovian process that should not be dependent on shorter time scales. C and τ define this final exponential decay. To minimize the number of floating parameters in the global fit, the final exponential is fit first using a single exponential decay at long time. This is repeated over multiple time ranges at long times to ensure the same value of the time constant is obtained. The reproducibility of the value of τ confirms that the fits are in the purely exponential region and are not being distorted by the von Schweidler power law. This time constant is then held constant in the initial global fit.

Simulation Methodology. Quantum chemistry *ab initio* calculations were first performed to obtain optimized molecular geometries of the $Ehim^+$ and $Emim^+$ cations, and their tightly bounded ion pair structures with the NTf_2^- anion, respectively, using the Gaussian 09 package[45] at B3LYP/6-311++g(d,p) level of theory.[46,47] The CHELPG[48] atomic partial charges on $Ehim^+$ and $Emim^+$ and NTf_2^- were calculated at the same level of theory (the B3LYP hybrid functional and the 6-311++G(d,p) basis set).

For the atomistic interaction parameters for the $EhimNTf_2$ and $EmimNTf_2$ ionic liquids, a procedure similar to that described in previous publications[49,50] was followed to develop force field parameters based on the AMBER framework. The SPC/E water model with constrained covalent bonds is employed in the current work. The cross interaction parameters between different atom types are obtained from Lorentz−Berthelot combination rules.

Preliminary atomistic simulations were performed on the $EhimNTf_2$ and $EmimNTf_2$ ionic liquids at various water concentrations to validate the force field parameters. The simulation procedures and parameters are described in the following in detail. The calculated liquid densities of two ionic liquids, as shown in Figure 2, are consistent with the experimental data within the water concentration range. This comparison indicates that the proposed force field parameters can properly describe phase behavior of the two types of ionic liquids, and thus are used to perform intensive atomistic simulations for $EhimNTf_2$ and $EmimNTf_2$ with varying water concentrations. The relative numbers of ion pairs and water molecules in each simulation system, as listed in Table 1, are determined to match the experimental RTIL/water mixture compositions.

Atomistic molecular dynamics simulations were performed using the GROMACS 5.0.4 package[51] with three-dimensional periodic boundary conditions. The equations of motion were integrated using a leapfrog integration algorithm with a time step of 1.0 fs. A cutoff radius of 1.6 nm was set for short-range van der Waals interactions and real-space electrostatic interactions. The particle-mesh Ewald summation method with an interpolation order of 5 and Fourier grid spacing of

DOI: 10.1021/acs.jpcb.7b06376
J. Phys. Chem. B XXXX, XXX, XXX−XXX

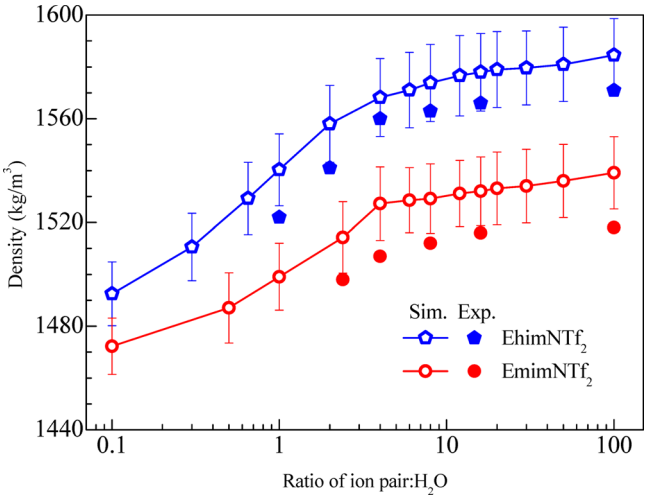

Figure 2. A comparison of liquid densities of EhimNTf$_2$ and EmimNTf$_2$/water mixtures calculated from atomistic simulations and experimental measurements at various water concentrations.

0.12 nm was employed to handle long-range electrostatic interactions in reciprocal space. All simulation systems were first energetically minimized using a steepest descent algorithm, and thereafter annealed gradually from 800 to 300 K within 10 ns. The annealed simulation boxes were equilibrated in the NPT (isothermal−isobaric) ensemble for 40 ns maintained using the Nosé−Hoover chain thermostat and the Parrinello−Rahman barostat with time coupling constants of 500 and 200 fs, respectively, to control the temperature at 300 K and pressure at 1 atm. Canonical ensemble simulations were further performed for 50 ns for all RTIL/water mixtures, and the simulation trajectories were recorded at an interval of 100 fs for further structural and dynamics analysis.

RESULTS AND DISCUSSION

Viscosity of Neat Ionic Liquids. Hydrogen bonding in the protic ionic liquid significantly alters the liquid structure even in the absence of water. This is readily apparent by comparing the viscosities of the two neat liquids, as given in Table 1. EhimNTf$_2$ is ∼1.5 times more viscous than EmimNTf$_2$. This is likely due to the ability of hydrogen atoms on the imidazolium ring of Ehim$^+$ to form stronger hydrogen bonds with the nitrogen and oxygen atoms in the NTf$_2^-$ anion than those in Emim$^+$. To verify this hypothesis, we calculated the combined distribution functions of ∠C/N−H···X versus the distances of H···X between Ehim$^+$/Emim$^+$ cations and NTf$_2^-$ anions from atomistic simulation trajectories. The hydrogen atoms are the ones bonded to carbon or nitrogen atoms of the imidazolium ring, including the H4 and H5 atoms in the two cations and the N−H moiety of Ehim$^+$, and X refers to O and N atoms in NTf$_2^-$ anions, respectively. The labeling of hydrogen atoms is shown on the chemical structure in Figure 1. The calculation results are given in Figure 3.

In EmimNTf$_2$, both the H4 (Figure 3I, H4···O) and H5 (Figure 3J, H5···O) atoms exhibit strong hydrogen bonding coordination with the O atoms in NTf$_2^-$; however, only the H5 atom (Figure 3E, H5···N) has prominent hydrogen bonding interactions with the N atoms of the NTf$_2^-$ anions. In EmimNTf$_2$, the H4 atom (Figure 3D, H4···N) has negligible coordination with the central N atoms in the neighboring NTf$_2^-$ anions due to its weak hydrogen bonding ability relative to the H5 atom.

Such a coordination feature is evident in Figure 4B which shows typical spatial distribution functions of N (solid blue surface) and O (meshed red surface) atoms in NTf$_2^-$ anions around a central Emim$^+$ cation. The O atoms in the NTf$_2^-$ anions show particular coordination to neighboring H4/H5 atoms on the imidazolium rings of the Emim$^+$ cation, indicating that the O atoms are localized in the first solvation shell of the H4 and H5 atoms and *vice versa*. The N atoms in the NTf$_2^-$ anions exhibit two distinct distribution domains along the CR-H5 vector, in which the one close to the H5 atom is overlapped with that for the O atoms. This contributes to the hydrogen bonding interactions between the H5 and N atoms. The second coordination region of N atoms around the H5 atoms and the distribution of N atoms around the CW-H4 vector are observed at further distances. These longer range interactions do not contribute to hydrogen bonding but are mainly due to the local chemical structure of the N and O atoms that are bonded to S atoms in the NTf$_2^-$ anions. The methyl and ethyl groups tend to exclude the N and O atoms of NTf$_2^-$ anions due to their hydrophobic nature.

In Ehim$^+$, the replacement of the methyl group by a hydrogen atom on the imidazolium ring leads to distinct hydrogen bonding coordination patterns of the N and O atoms

Table 1. OKE, Viscosity, and Simulation Parameters for EmimNTf$_2$/Water and EhimNTf$_2$/Water Solutions

	experimental data					simulation parameters		
	ion pair:water	water mole fraction	τ (ps)	viscosity (cP)[a] (24.4 °C)	friction	no. of ion pairs	no. of water molecules	total no. of atoms
EmimNTf$_2$	dry	0	376 ± 11	36.3	1.42 ± 0.01	370	0	12580
	16:1	0.059	290 ± 8	28.9	1.38 ± 0.01	360	23	12309
	8:1	0.111	263 ± 6	26.0	1.39 ± 0.01	360	45	12375
	4:1	0.200	239 ± 5	21.9	1.49 ± 0.01	360	90	12510
	2.6:1	0.278	184 ± 6	18.2	1.39 ± 0.01	360	150	12690
EhimNTf$_2$	dry	0	491 ± 14	57.1	1.53 ± 0.01	400	0	12400
	16.1	0.059	429 ± 9	50.8	1.50 ± 0.01	400	25	12475
	8:1	0.111	367 ± 8	44.9	1.46 ± 0.01	400	50	12550
	4:1	0.200	287 ± 3	32.7	1.56 ± 0.01	392	98	12446
	2:1	0.333	194 ± 3	24.1	1.43 ± 0.01	384	192	12480
	1:1	0.500	175 ± 7	15.8	1.97 ± 0.02	370	370	12580
	0.65:1	0.641	119 ± 8	11.2	1.89 ± 0.02	350	540	12470

[a]Error bars are within ±1%

DOI: 10.1021/acs.jpcb.7b06376
J. Phys. Chem. B XXXX, XXX, XXX−XXX

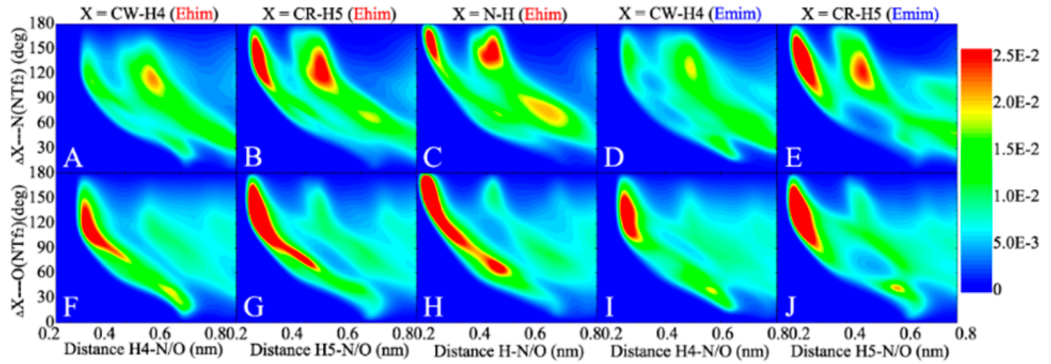

Figure 3. Combined distribution functions of ∠C/N−H···N/O versus the distance of H···N/O between the $Ehim^+$/$Emim^+$ cations and NTf_2^- anions in the two neat ionic liquids. Panels A−E look at interactions with the N in NTf_2^- (∠C/N−H---N) while panels F−J look at interactions with the O in NTf_2^- (∠C/N−H---O.) Panels A−C and F−H are combined distribution functions for $EhimNTf_2$. Panels D−E and I−J are combined distribution functions for $EmimNTf_2$.

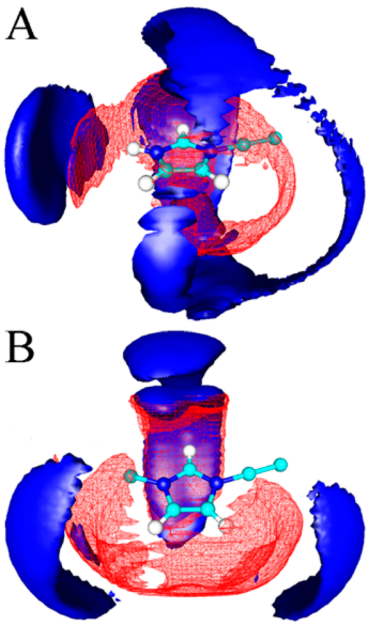

Figure 4. Three-dimensional probability distributions of N (solid blue surface) and O (meshed red surface) atoms in NTf_2^- anions around (A) $Ehim^+$ and (B) $Emim^+$ cations in the neat ionic liquids obtained from atomistic simulations at 300 K. In each case, the solid blue and meshed red contour surfaces are drawn at 4.0 times the average density of corresponding atoms in the bulk region.

in NTf_2^- anions around $Ehim^+$ cations, as shown in the six leftmost panels of Figure 3. The H4 and H5 atoms in the $Ehim^+$ cations have comparable hydrogen bonding interactions with the N and O atoms of the NTf_2^- anions as those with $Emim^+$ cations, as clearly shown in Figure 3A (H4···N), 3B (H5···N), 3F (H4···O), and 3G (H5···O), respectively. The H atom of the N−H of the $Ehim^+$ cation exhibits stronger coordination with O atoms (Figure 3H) than N atoms (Figure 3C) in the first solvation shell, but shows the opposite feature in the second solvation shell in coordinating neighboring NTf_2^- anions. The spatial distribution functions shown in Figure 4A indicate that the O atoms in the NTf_2^- anions prefer to form multiple hydrogen bonds with all hydrogen atoms (H4, H5 and N−H) on the imidazolium rings leading to their diffusive feature around the imidazolium ring in the $Ehim^+$ cation. The N atoms in the NTf_2^- anions are mainly localized around the N−H and H5 sites, thus resulting in their discrete distributions near H4 atoms. It should be noted that the F atoms in the NTf_2^- anions are not involved in intermolecular hydrogen bonding interactions. The formation of a hydrogen bond network between the $Ehim^+$ cations and the NTf_2^- anions with multiple varying magnitudes of interactions tightens the local ionic structure and therefore contributes to slowing the diffusion of the $Ehim^+$ cations in the ionic liquid matrix. This hydrogen bonding network is of greater magnitude and complexity than that seen in $EmimNTf_2$. This microstructural change contributes to $EhimNTf_2$ having a greater viscosity than $EmimNTf_2$ and affects other dynamical properties as discussed in the following subsections.

OHD-OKE. Before analyzing the OHD-OKE data, one must consider which parts of each sample are contributing to the signal. In the samples studied here, there are water, anions, and cations. OHD-OKE measures the derivative of the polarizability-polarizability correlation function, which is akin to the orientational correlation function, after very early time. Thus, any molecule with anisotropic polarizability will contribute to the signal. Water does not have significant anisotropic polarizability relative to the ionic liquid, so its contribution is negligible after very early time.[52−54] Thus, the signal is dominated by the RTIL, and we can analyze which RTIL structural features have the most significant contributions. In previous OHD-OKE studies of imidazolium-based ionic liquids, the corresponding anions, Cl^- and BF_4^-,[22,23] did not have single particle polarizability anisotropy. Very short time collision-induced interactions can generate a small polarizability anisotropy, but at longer times, ions like these will have zero contribution to the signal. The asymmetric NTf_2^- anion will have an anisotropy polarizability; the question is how large is it compared to the imidazolium. The Wynne group calculated the square of the derivative of the polarizability anisotropy for imidazolium NTf_2^- ionic liquids.[36] The results demonstrated that the contribution of the NTf_2^- anions to the signal is negligible relative to the signal produced by the imidazolium cations. Therefore, the OHD-OKE experiments are essentially comparing the motions of the $Emim^+$ and $Ehim^+$ cations.

The OHD-OKE decays for $EmimNTf_2$ at five water concentrations and $EhimNTf_2$ at seven water concentrations are plotted in Figure 5. The data have been vertically offset for clarity and both axes are logarithmic. All decays have been fit using eq 1, and a sample fit is shown by a dashed red curve through the data for the water saturated $EmimNTf_2$ sample (Figure 5A, bottom curve). Fits of the data for all samples were

DOI: 10.1021/acs.jpcb.7b06376
J. Phys. Chem. B XXXX, XXX, XXX−XXX

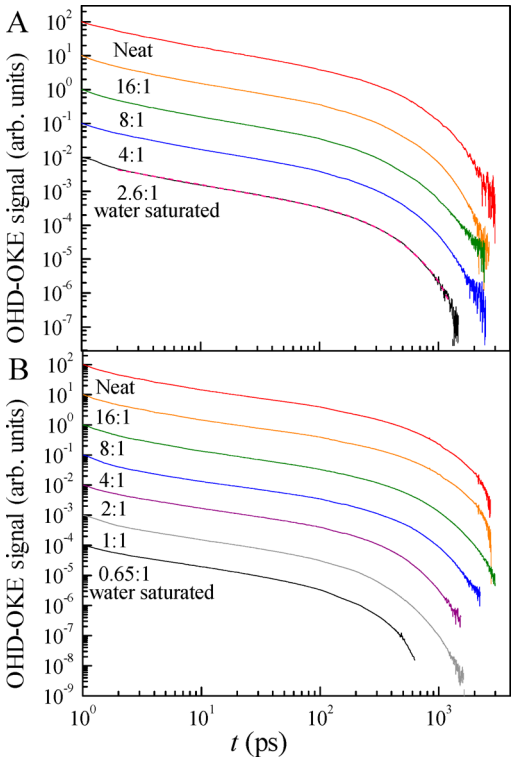

Figure 5. OHD-OKE data for (A) $EmimNTf_2$ and (B) $EhimNTf_2$ at various water concentrations ranging from dry (red) to water saturated (black). The data are vertically offset for clarity. A sample fit using eq 1 is shown by the dashed line on the saturated $EmimNTf_2$ data. Fits of all data sets were of similar quality.

of similar quality. For both ionic liquids, the value of b is independent of water concentration which suggests that the addition of water does not affect the short time caged motions of the ions. However, the change in cation did slightly impact the value of b. For $EmimNTf_2$, b = 0.61 ± 0.01 while, for $EhimNTf_2$ b = 0.58 ± 0.02. The difference, which is on the edge of overlapping error bars, may suggest that the nondiffusive dynamics are slightly different in the two liquids.

The power law region precedes a single exponential for all the samples measured. In previous OHD-OKE studies of imidazolium-based ionic liquid/water solutions,[22,23] biexponential decays were observed at high water concentrations for cations with long alkyl chains. The biexponentials occurred as the systems approached the formation of gels at high water concentration. Single exponential decays were observed here for two reasons. First, the ethyl chain off the imidazolium is not long enough to have an apolar region in the liquids, which was necessary for gel formation.[22,23] Second, NTf_2^- ionic liquids become water saturated before the concentration range where biexponential decays were observed previously. The final single exponential time, τ, which describes the complete randomization of the cations, shows a clear water concentration dependence that can be systematized by comparing the results to changes in the viscosity. Values of τ are given in Table 1.

Increasing the water concentration in RTILs usually decreases the viscosity because the water infiltrates the ionic regions and decreases the Coulombic attraction of the cations and anions. This weakened attraction allows the molecules to move more readily and the viscosity to decrease.[55] This expected trend is seen in both $EmimNTf_2$ and $EhimNTf_2$. For samples that display hydrodynamic behavior, the viscosity is related to the final exponential measured in the OHD-OKE experiment by the generalized Debye–Stokes–Einstein (DSE) equation which is given as eq 2

$$\tau_{self} = \frac{\eta(T) V f_\theta C}{k_B T} \tag{2}$$

where τ_{self} is the rotational self-diffusion time for a symmetric top, η is the shear viscosity, V is the molecular volume, k is the Boltzmann constant, and T is the temperature. The parameter f_θ is a shape factor used to account for the deviation from sphericity of the rotator. Its functional form has been calculated by Perrin[56] and ranges from 1 for a perfectly spherical rotator to increasingly greater than 1 as the rotator becomes more elongated. C is an interaction factor that accounts for the interaction of the rotator with adjacent molecules.[57] C ranges from 0 for a sphere under slip boundary conditions to 1 for any rotator under stick boundary conditions, Together, C and f_θ describe the friction experienced by the rotator.

τ_{self} can be related to τ, the bulk diffusion measured with OHD-OKE and other experiments. The relationship is given in eq 3

$$\tau = \frac{g_2}{j_2}\tau_{self} \tag{3}$$

where g_2 is the static orientational correlation factor and j_2 is the dynamic orientational correlation function. g_2 is often taken to be 1 for isotropic phases where there is no time independent orientational correlation as would be found, for example, in the nematic phase of a liquid crystal. j_2 has been shown to be approximately 1 for a multitude of liquids.[58–60] Thus, in most cases, eq 2 can be used without modification to describe bulk dynamics.

To test whether the RTIL/water mixtures obey eq 2, the final exponential time was plotted versus viscosity in Figure 6. The

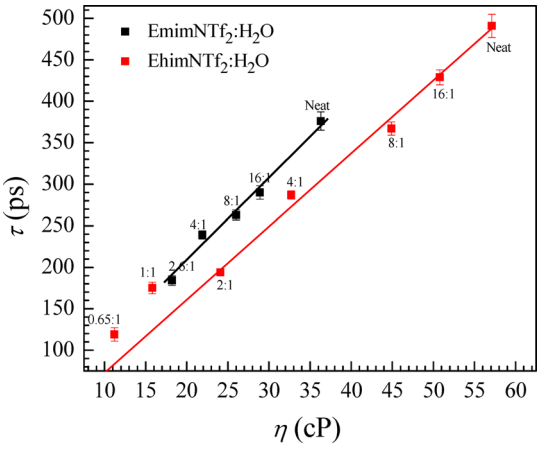

Figure 6. Debye–Stokes–Einstein plot for $EmimNTf_2$/water mixtures (black) and $EhimNTf_2$/water mixtures (red). Lines are linear fits to the data. For $EhimNTf_2$ fits were from the neat through 2:1 samples only.

lines are fits to the $Emim^+$ data (black) and the 5 lowest water content $Ehim^+$ data points (red). The red line was extended. For the $EmimNTf_2$ samples, all the time constants fall on a line, indicating that $EmimNTf_2$/water mixtures exhibit DSE (hydrodynamic) behavior and that the addition of water does not fundamentally alter the nature of the dynamics experienced by

DOI: 10.1021/acs.jpcb.7b06376
J. Phys. Chem. B XXXX, XXX, XXX–XXX

the cation. The rotational diffusion times (as measured by OHD-OKE) decreased linearly with the decrease in viscosity. The plot for $EhimNTf_2$ displays linear behavior through the 2:1 sample as shown by the red line. However, the 1:1 sample and the saturated sample do not fall on the hydrodynamic line. The red line has been extended beyond the data points to help visualize the deviation. This deviation from linearity occurs at the viscosity where $EmimNTf_2$ reaches its saturation point. It should be noted that this deviation from hydrodynamic behavior has not been observed in short-chained aprotic ionic liquids that can reach <2:1 concentration.[23] This deviation suggests that the protic nature of the $Ehim^+$ cation alters its interactions with water molecules. As discussed in detail below, there is a significant change in the manner in which water interacts with the protic ionic liquid between the 2:1 $EhimNTf_2$:water and the 1:1 $EhimNTf_2$:water solutions. This change results in slower dynamics than expected from the bulk viscosity and the DSE equation, and also allows more water to be added before reaching the saturation point.

Another interesting result from this plot is that while the slopes of both lines in Figure 6 are the same within experimental error, the intercept for $EmimNTf_2$ is actually larger. This means that an $EmimNTf_2$/water sample, at the same viscosity as an $EhimNTf_2$/water sample, will actually undergo orientational randomization more slowly despite the ability of $Ehim^+$ to form strong hydrogen bonds with water resulting in a greater value of C in eq 2. The relatively slow orientational relaxation of an $Emim^+$ sample compared to $Ehim^+$ at the same viscosity may be caused by the $Emim^+$ methyl group that increases the volume (V) as well as the shape factor (f_θ) due to the increased elongation of the rotator. It should be noted that significantly more water must be added to $EhimNTf_2$ to reach the same viscosity.

It is clear from the DSE plots (Figure 6) that viscosity greatly influences the dynamics of the system. Another way of analyzing the data is by calculating friction, which provides information on changes in liquid structure independent of viscosity. The friction coefficient for rotation about the i^{th} axis, λ_i, is given by

$$\lambda_i = \frac{kT}{\eta V D_i} \tag{4}$$

where k is the Boltzmann constant, T is the temperature, V is the volume of the rotator, η is the viscosity, and D_i is the orientational diffusion coefficient. The diffusion coefficient is equal to $1/6\tau$ where τ is the final randomization time constant from fitting the data with eq 1. Since the cation is the source of most of the OHD-OKE signal, the $Emim^+$ and $Ehim^+$ cations are the rotators for these calculations.

Friction coefficients are often compared to theoretical slip and stick boundary conditions. Slip boundary conditions generally apply to a rotating molecule that is small compared to the solvent. The small molecule does not drag solvent molecules with it when it rotates. Friction arises from a nonspherical molecule's swept volume as solvent has to move out of the way of the rotator. Stick boundary conditions generally apply when the rotating molecule is comparable in size or large compared to the solvent molecules; the rotator is dragging other molecules with it as it rotates and this is the source of friction. Molecules with friction coefficients between the two extremes have contributions from both sources of friction.

Theoretical dimensionless frictional coefficients have been tabulated for slip boundary conditions for oblate and prolate spheroids as a function of the axis ratio, ρ.[61,62] To determine ρ, both cations were modeled as prolate spheroids. For $Emim^+$, the long axis was calculated as the nuclear distance between the farthest hydrogen atom on the ethyl group and the farthest hydrogen on the methyl group plus two times the hydrogen van der Waals radius. In $Ehim^+$, the long axis was determined in the same manner except for a hydrogen atom replaced the methyl group. The van der Waals radius for a hydrogen atom in a C−H bond is 1.09 Å.[63] The short axis of both cations was determined to be the component of the distance between the hydrogen atoms bound to CR and CW (as labeled in Figure 1) that is perpendicular to the long axis. Again, van der Waals radii were taken into account. This procedure resulted in volumes similar to the volumes obtained from quantum chemical calculations. For $Emim^+$, the long axis was 9.94 Å and the short axis was 6.00 Å. This resulted in $\rho = 0.60$. The tabulated friction coefficient was $\lambda_{slip} = 1.13$ for a prolate spheroid with $\rho = 0.60$ under slip boundary conditions.[61,62] For $Ehim^+$, the long and short axes were 8.74 and 6.00 Å, respectively. The axis ratio was determined to be $\rho = 0.69$ which resulted in $\lambda_{slip} = 0.61$ for slip boundary conditions. By comparing eqs 2 and 4, it is clear that $\lambda_i = 6f_\theta C$. For a rotator under stick boundary conditions, $C = 1$,[57] so λ_{stick} can be determined through the calculation of the shape factors using the Perrin equations.[56] The λ_{stick} value is 7.02 for $Ehim^+$ and 7.74 for $Emim^+$, respectively.

To calculate the experimental friction coefficients, the volume of each cation was taken from simulations. This volume, along with experimental values of η, τ, and T were used to calculate friction coefficients with eq 4. The results are given in Table 1. For both cations, the experimental friction coefficients are much closer to λ_{slip} than to λ_{stick} but fall between the two extremes. To compare the two cations, λ was then normalized to λ_{slip}. This allowed the deviation from slip boundary conditions to be compared, and these results are plotted in Figure 7. The dashed lines are horizontal fits to the $Emim^+$ data (black) and the 5 lowest water content $Ehim^+$ data points (red). The red line was extended. Although the points jump around to some extent, for $EmimNTf_2$, the friction

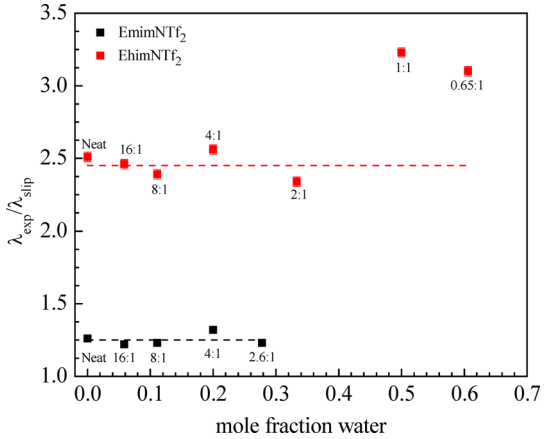

Figure 7. Friction normalized to the friction under slip boundary conditions is plotted as a function of water content for $EmimNTf_2$ (black) and $EhimNTf_2$ (red). The theoretical friction coefficient under slip boundary conditions is 1 on this plot. The dashed lines are horizontal fits to the data. For $EhimNTf_2$ fits were from the neat through 2:1 samples only.

DOI: 10.1021/acs.jpcb.7b06376
J. Phys. Chem. B XXXX, XXX, XXX−XXX

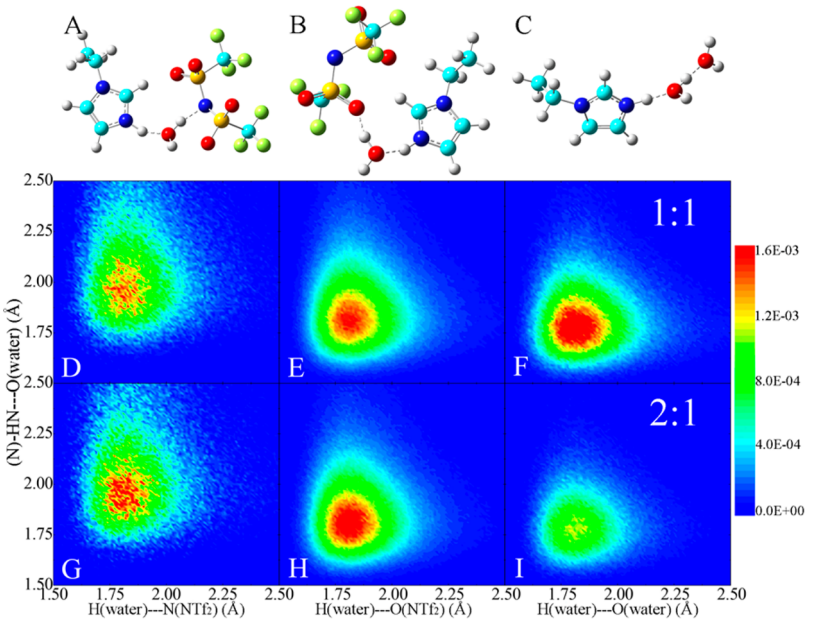

Figure 8. Combined distribution functions of the distance of N−H···O(water) between a reference water molecule and a neighboring $Ehim^+$ cation versus the distance of water O−H···N/O between the reference water and neighboring NTf_2^- anion. A−C show typical ionic structures of $Ehim^+$,H_2O, an NTf_2^- complexes. The distribution functions in D−F and G−I are obtained from $EhimNTf_2$ ionic liquid/water mixtures with the ion pair:water ratio of 1:1 and 2:1, respectively. Panel F shows the onset of water−water hydrogen bonds at an ion pair/water concentration of 1:1.

coefficients remain essentially constant regardless of water content, which is expected for a liquid that obeys the DSE equation, i.e., it behaves in accord with hydrodynamics. As discussed above, the OHD-OKE experiment mainly measures the orientational relaxation of the cation. However, $Emim^+$ will interact strongly with neighboring ionic species as reflected by the deviation of λ from λ_{slip}. The details of the interactions are discussed below. The constant friction coefficient with varying water content demonstrates that water does not change the essential nature of local ionic structures in $EmimNTf_2$ RTIL/water mixtures.

The situation is quite different for $EhimNTf_2$. The friction coefficients deviate from slip boundary conditions more significantly than those for $Emim^+$, but they are basically constant, within the scatter, up to an ion pair/water ratio of 2:1. So for the lower water concentrations, $Ehim^+$ like $Emim^+$ experiences little change in nature of its interactions with neighboring species in the ionic liquids. The increase in the friction coefficient for $Ehim^+$ relative to $Emim^+$ is related to the differences in hydrogen bonding. As discussed in connection with the viscosity in the Viscosity of Neat Ionic Liquids Section, the N−H group in $Ehim^+$ readily hydrogen bonds with both the N and O atoms of the anion. Since $Emim^+$ lacks a strong hydrogen bond donor, it interacts more weakly with the anion. The increase in hydrogen bonding between $Ehim^+$ and NTf_2^- can lead to greater friction.

However, for the samples with more water (1:1 and 0.65:1) there is a large jump in the $Ehim^+$ friction coefficients that is well outside of experimental error. This sudden change corresponds to the deviation from the DSE hydrodynamic behavior in Figure 6 (red line) at high water content. The substantial increase in friction coefficients when the sample reaches 1:1 ion pair:water demonstrates a fundamental change in the manner in which the $Ehim^+$ cation interacts with neighboring ionic groups in its local environment. Since the friction coefficients move further away from the slip boundary condition, it suggests that the cation is experiencing stronger interactions with the surrounding ions. This result leads to questions of what interactions $Ehim^+$ experiences and how water impacts these interactions, particularly what changes at the 1:1 concentration. To answer these questions, atomistic simulations of the two ionic liquids were conducted for the range of water concentrations studied experimentally to investigate the detailed changes of local microscopic ionic structures upon increasing the water concentration in the ionic liquid/water mixtures.

Atomistic Simulations. In the $EhimNTf_2$ RTIL/water mixtures, the atomistic simulation results demonstrate that water molecules preferentially reside in cavities between the $Ehim^+$ cations and the NTf_2^- anions. The dispersed distribution of water among ionic species tends to break the directional hydrogen bonds between the $Ehim^+$ cations and the NTf_2^- anions, and thereafter form new hydrogen bonds between water molecules and neighboring ionic species, as shown in the typical ionic structure of the $Ehim\cdots H_2O\cdots NTf_2$ complex in A and B of Figure 8. The O atoms in water molecules are strongly coordinated with hydrogen atoms that are directly bonded to the imidazolium ring in the $Ehim^+$ cations. In addition, the hydrogen atoms of these same water molecules are weakly hydrogen bonded to the N and O atoms of neighboring NTf_2^- anions. Water molecules serve as a bridge between the $EhimNTf_2$ ion pairs previously in close contact. This complicates the local ionic environment as increasing amounts of water are added, resulting in new hydrogen bond networks forming among ionic groups.

In the 2:1 $EhimNTf_2$:water sample, almost all water molecules are isolated single molecules located between $Ehim^+$ cations and neighboring NTf_2^- anions. The further introduction of water molecules into this sample leads to the distinct aggregation of water molecules in ionic cavities. As discussed below, water−water hydrogen bonds are observed in the $EhimNTf_2$/water sample with the ratio of 1:1 ion

DOI: 10.1021/acs.jpcb.7b06376
J. Phys. Chem. B XXXX, XXX, XXX−XXX

pair:water. This observation indicates that in the $EhimNTf_2$ samples both dispersed water molecules and small water aggregates tend to reside in pockets between neighboring ionic species. This computational result is consistent with that observed in $BmimNO_3$-D_2O samples with small-angle X-ray scattering and neutron scattering experiments.[64] This observation is in contrast to many nonionic liquids with hydrogen bonding capabilities. For instance, OHD-OKE and 2D IR spectroscopy have been used to study binary mixtures of dimethyl sulfoxide (DMSO) and water.[65] This study demonstrated that even at very low water concentrations, water−water hydrogen bonds and the formation of water clusters were preferred over the water molecules being widely dispersed and hydrogen bonding mainly to DMSO.

The lack of formation of water−water hydrogen bonds in the low water concentration $EhimNTf_2$ solutions shows that the hydrogen bonding to the ions, particularly bonding of the water oxygen to the nitrogen-bound hydrogen atom of $Ehim^+$ is comparable in strength to the bonding of a water hydroxyl to a water oxygen. At low water content, the number of N−H groups substantially outnumbers the water hydroxyls; therefore the water oxygens will be bound to the H atoms of the N−H moiety. The hydroxyl groups will make weak hydrogen bonds to the neighboring NTf_2^- anions. However, for the 1:1 mixture, if the hydrogen bonding of the H of N−H to a water oxygen is approximately equally favorable as the oxygen bonding to another water's hydrogen, statistically there will be a significant number of water−water hydrogen bonds. For no water−water hydrogen bonds to form in the 1:1 mixture, every water oxygen would have to be bound to every N−H in every $Ehim^+$ cation. This would only occur if the oxygen hydrogen bonding to these Hs was overwhelmingly more favorable than bonding to another water hydroxyl. The other extreme would be that forming a water−water hydrogen bond is vastly more favorable than the bonding of the water oxygen to the H of N−H; then, water−water hydrogen bonds would form at low water concentrations as happens in DMSO.

To characterize the local ionic structural changes in $EhimNTf_2$ as the water concentration increases from 2:1 to 1:1, the combined distribution functions of the distance of (N)-H···O(water) versus the distances of H(water)···N(NTf_2^-), H(water)···O(NTf_2^-), and H(water)···O(water) were calculated. Schematic molecular structures and distribution functions are shown in Figure 8. Figure 8D and 8G shows these distribution functions for a single water molecule embedded between a close contact $Ehim^+$ cation and the nitrogen atom in the NTf_2^- anion as illustrated in Figure 8A. During statistical analysis, both the cis and trans conformations of the NTF_2^- anions in coordination with the $Ehim^+$ cations were considered. Figure 8E and H shows the combined distribution functions for a single water molecule confined between an $Ehim^+$ cation and the oxygen atoms in a neighboring NTf_2^- anion as displayed in Figure 8B. The distribution features are comparable in these two $EhimNTf_2$ ionic liquid/water mixtures showing that these structures do not make a substantial change in going from 2:1 to 1:1. However, increasing the water concentration from 2:1 to 1:1 ion pair:water, there is a dramatic change as is seen by comparing Figure 8I to Figure 8F. There are few water−water hydrogen bonds in 2:1 sample (Figure 8I), but a substantial increase in the number of water−water hydrogen bonds is observed in the 1:1 sample (Figure 8F). The water−water hydrogen bonding is illustrated in Figure 8C. These results indicate that the break in the nature of the dynamics in going from 2:1 to 1:1 ion pair:water shown in Figure 6 (orientational relaxation time constants) and Figure 7 (friction coefficients) is caused by the abrupt onset of water−water hydrogen bonding between dispersed water molecules in the local ionic environment.

When a water−water hydrogen bond forms, as shown in Figure 8C, one hydroxyl of the water that has its oxygen bound to the H atom of the N−H moiety makes a hydrogen bond to another water. For these two water molecules, the remaining three hydroxyls will make hydrogen bonds to neighboring NTf_2^- anions. The quantum chemistry simulations show that the oxygen H-bond to the H (N−H···O) becomes stronger when one of the water's hydroxyl groups is H-bonded to another water molecule. The increase in strength is shown by the decrease in length of the H-bond. When there is a single water molecule, the H-bond length of N−H···O is ∼1.7 Å. However, when the hydroxyl of this water oxygen is bound to another water oxygen rather than to a neighboring NTf_2^- anion, the N−H···O hydrogen bond length is reduced to 1.64 Å. This substantial decrease in length indicates a significant increase in the H-bond strength.

The OHD-OKE experiment essentially measures the orientational relaxation of the $Ehim^+$ cations. In the absence of water, the $Ehim^+$ cations directly interact with surrounding NTf_2^- anions. Figure 7 shows that for $Emim^+$ and $Ehim^+$ at the lower water concentrations, the friction coefficients are closer to slip boundary conditions than stick boundary conditions. The reorientation of a cation does not involve dragging large clusters of ions with it. At low water content, some close contact ion pairs will be separated by a single water molecule. When a single water molecule intervenes, the Coulombic interactions between ions are reduced, but hydrogen bonding occurs. The reduction in the Coulombic interactions replaced by weak hydrogen bonding results in faster cation reorientation. Comparing Figures 8I and 8F, the onset of water−water hydrogen bonding occurs at ∼1:1 concentration. This is the concentration at which the reorientational dynamics of $Ehim^+$ cations slow relative to what would be predicted by hydrodynamics as shown in Figures 6 and 7. With the formation of water−water hydrogen bonds, the H-bonding of the H of the N−H moiety of $Ehim^+$ to water becomes stronger and there are strong H-bonds between water molecules. These water pairs and clusters, which will be even more prevalent at the 0:65:1 concentration, will further reduce the Coulombic interactions among cations and anions, lowering the overall viscosity. However, it is likely to make it more difficult for the $Ehim^+$ cations to break free from the water hydrogen bond network, causing the cation orientational relaxation not to speed up as much as would be expected from the decrease in viscosity.

Linear Infrared Spectra. Additional information that sheds light on the structural changes in the $EhimNTf_2$ PIL as water is added can be obtained from FT-IR spectra. This also helps validate results of the simulations. As discussed in the Sample Preparation Section, the N−H was partially deuterated (5%) and then 5% HOD in H_2O was added to make the IL-water mixtures. By using 5% HOD, the N-D concentration was not changed with the addition of water and a single O−D local mode of the water could be observed, which somewhat simplified the complex spectrum of the N-D/O−D stretching modes. For each spectrum, the equivalent nondeuterated spectrum was subtracted to yield, within subtraction error, only the deuterated peaks.

DOI: 10.1021/acs.jpcb.7b06376
J. Phys. Chem. B XXXX, XXX, XXX−XXX

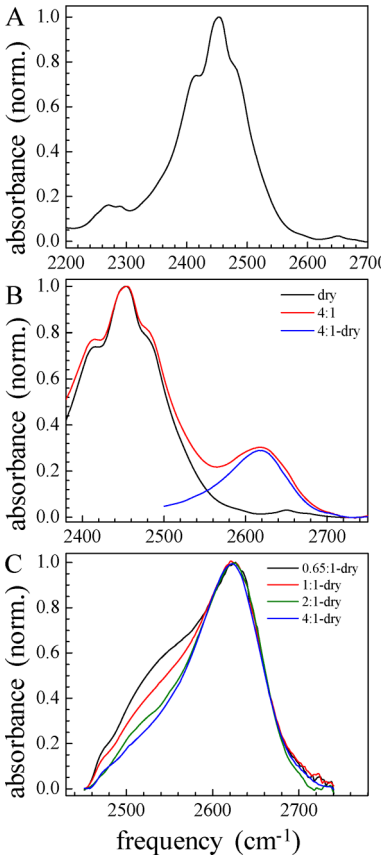

Figure 9. Background-subtracted FT-IR spectra of the N-D stretch of 5% D Ehim-DNTf$_2$ and with the addition of 5% HOD/H$_2$O. (A) The dry spectrum of the imidazolium N-D stretch shows several overlapping bands caused by the multiple hydrogen bonding configurations of the N-D with the anion. (B) The red curve shows the spectrum of the 4:1 ion pair/water concentration. The blue curve is the spectrum after subtraction of the dry spectrum (black curve). Lower water concentrations show the same feature as the blue curve but with lower amplitude. (C) Normalized spectra with the dry spectrum subtracted for four ion pair/water concentrations: 4:1 (blue), 2:1 (green), 1:1 (red), and 0.65:1 (black). At 1:1, a new broad shoulder appears on the red side of the line that is attributed to the onset of the OD stretch of HOD hydrogen bonded to the oxygen of another water molecule.

Figure 9A is the spectrum of dry Ehim-DNTf$_2$. The main band is the N-D stretching mode. The spectrum has three components but is most likely composed of at least four overlapping bands. The simulations show that in the absence of water, the N-D will be weakly H-bonded to the NTf$_2^-$. It has been previously shown that the NTf$_2^-$ ion has cis and trans conformations in the liquid phase.[66] In addition, from the current quantum chemical simulations, four configurations were identified, N-D bound to either oxygen or nitrogen in the cis or trans configurations of the NTf$_2^-$ anions. These four configurations have different H-bond strengths which will shift the N-D stretch frequency. A shorter hydrogen bond is stronger. A stronger H-bond will shift the N-D stretch further to the red (low frequency). The quantum chemical calculations with explicit inclusion of empirical dispersion terms show that the hydrogen bonding interaction between the N-D site and the O atoms in neighboring NTf$_2^-$ anions in the cis conformation is about the same strength as that in the trans conformation. These two types of hydrogen bonding interactions are weaker than the coordination of the H atom of the N−H moiety to the nitrogen atom of a neighboring NTf$_2^-$ anion. Additionally, the H-bond formed between the H atom and the nitrogen atom in the NTf$_2^-$ anion with the trans conformation is much stronger than it is with the cis conformation. From these qualitative considerations, the blue shoulder may be overlapping N-D stretches with deuterium hydrogen bonded to the oxygen atom in either the cis or trans conformation of the NTf$_2^-$ anion. The central peak is the N-D stretch bound to the nitrogen in the cis conformation of NTf$_2^-$ and the red shoulder is for the trans NTf$_2^-$ configuration.

Figure 9B shows spectra of the dry sample (black), the 4:1 sample (red), and the result of subtracting the dry spectrum from the 4:1 spectrum (blue). The blue-colored band occurs once HOD/H$_2$O is added. It is centered at ∼2625 cm^{-1}. Note that the band is not symmetrical. It is broader on the red side of the spectrum. As the amount of water is increased from 16:1 to 4:1, the band amplitude increases linearly with water concentration within error. The blue-colored band in Figure 9B is the OD stretch of HOD weakly hydrogen bonded to the NTf$_2^-$. This type of band has been observed previously when HOD is added to other ionic liquids. The OD stretch in 1-butyl-3-methylimidazolium hexafluorophosphate (BmimPF$_6$) has a peak position of 2678 cm^{-1}.[67] The band is symmetrical. The OD hydrogen bond is very weak as shown by the very high frequency of the stretching mode. For comparison, the OD stretch of HOD in bulk H$_2$O peaks at 2509 cm^{-1}.[68] The OD stretch of HOD in EmimNTf$_2$ is at 2648 cm^{-1} and is somewhat broader on the red side of the band.[69] The OD stretch in EmimBF$_4$ has its peak at 2645 cm^{-1}.[70] This band is symmetrical at very low water concentrations. As the water concentration is increased a broad band grows in centered at ∼2550 cm^{-1}. This band arises from ODs H-bonded to the oxygen of water molecules in the mixture with the RTIL. Stronger H-bonds red shift the OD stretch. The observed OD stretch in EhimNTf$_2$ compared to EmimNTf$_2$ shows that the OD H-bond to the NTf$_2^-$ is somewhat stronger when the cation is Ehim$^+$ than Emim$^+$. The asymmetry of the band is likely caused by the variety of H-bonding sites to NTf$_2^-$ compared to PF$_6^-$ or BF$_4^-$.

Figure 9C displays the spectra of the Ehim-DNTf$_2$/water mixtures for four ion pair:water mixtures with the dry spectrum (Figure 9A) subtracted. The concentrations are 0.65:1, 1:1, 2:1, and 4:1. The 4:1 spectrum in Figure 9C is the same as the blue curve in Figure 9B. The 16:1 and 8:1 spectra with the dry spectrum subtracted look the same as the 4:1 spectrum (blue) except for their amplitudes, which increase with increasing water concentration. The important feature of Figure 9C is the large wing on the red side of the line for the 0.65:1 and 1:1 spectra. In a study of water dynamics in 1-alkyl-3-methylimidazolium tetrafluoroborates as a function of alkyl chain length and water concentration,[70] at low water content there is a narrow symmetric peak 2645 cm^{-1} from the OD stretch of HOD bound to the BF$_4^-$. As the water concentration is increased a broad band grows in on the red side of this peak. This peak becomes very large at the high water concentrations that are possible in EmimBF$_4$/water mixtures because the components are infinitely miscible. This band arises from OD bound to the oxygen of another water molecule. For EmimBF$_4$ at a 1:1 water concentration, the broad band is ∼35% in amplitude of the 2645 cm^{-1} peak and is centered at ∼2540 cm^{-1}. In EmimBF$_4$, the 2645 cm^{-1} peak is relatively narrow and symmetric resulting in the broad band being quite well resolved. For EhimNTf$_2$, the band overlaps substantially with

DOI: 10.1021/acs.jpcb.7b06376
J. Phys. Chem. B XXXX, XXX, XXX−XXX

the peak at 2625 cm^{-1} and is not well resolved. The peak of the broad shoulder is located at ~2625 cm^{-1}.

The important aspect of the data is that the broad feature is akin to that observed in the $EmimBF_4$/water study. We, therefore, assign the broad feature in the 1:1 and 0.65:1 spectra as arising from the OD stretch of HOD bound to the oxygen of another water molecule. While there may be an initial change in the 2:1 spectrum centered around 2500 cm^{-1}, this may also be an artifact of the several spectral subtractions needed to obtain the spectra. The major change in the spectra occurs at the 1:1 water mixture and increases in the 0.65:1 mixture. The 1:1 concentration where the broad feature appears is consistent with the simulation results (see Figure 8) that show the abrupt onset of water−water hydrogen bonding at the 1:1 water concentration. This concentration is also the concentration at which there is a discontinuity in the nature of the dynamical data shown in Figures 6 and 7. Thus, three methods confirmed that a significant change occurs at the 1:1 concentration. As argued above, the structural change evidenced in the FT-IR spectra and the simulations is responsible for the dynamical change observed in the OHD-OKE data.

CONCLUDING REMARKS

Protic ionic liquids are an increasingly important area of study due to their many applications throughout the fields of energy, biochemistry, and synthesis. Their relatively hygroscopic nature means that studying their interactions with water is useful because maintaining dry ionic liquids on an industrial scale is generally exceedingly costly both in time and money. Additionally, in energy applications, water has been shown to be a beneficial cosolvent due to its ability to decrease ionic liquid viscosity. In this work, we have used three methods to study a protic ionic liquid, $EhimNTf_2$, and its structurally analogous aprotic counterpart, $EmimNTf_2$. The liquid structure of both ionic liquids was investigated at water concentrations ranging from dry to saturated.

Optical heterodyne-detected optical Kerr effect experiments were used to examine the orientational dynamics from picoseconds to nanoseconds. FT-IR spectra were used to examine the hydrogen bonding of the N-D group in the deuterated $Ehim^+$ cation. The experimental data were complemented by atomistic simulations that provided increased insights into the intermolecular interactions experienced by both cations.

All three methods showed a dramatic change in liquid structure in $EhimNTf_2$ between the 2:1 ion pair:water and 1:1 solutions. Friction coefficients calculated from the OHD-OKE data showed that $EmimNTf_2$ exhibited hydrodynamic behavior at all water concentrations. $EhimNTf_2$ was also hydrodynamic up to the 2:1 concentration, although the friction coefficients were somewhat higher than those observed in $EmimNTf_2$. The difference was caused by the ability of $Ehim^+$ to make a reasonably strong hydrogen bond with the NTf_2^- anion. This was confirmed by atomistic simulations. At 1:1, the $EhimNTf_2$ friction coefficient increased greatly, which was indicative of a significant structural change. The N-D peak of the FT-IR spectrum remained largely unchanged for all spectra drier than 2:1. Once the 1:1 concentration was reached, an additional broad band appeared and became larger at higher concentrations. In analogy with previous studies of water in RTILs, this band is assigned to the onset of the formation of water−water hydrogen bond. Atomistic simulations showed that 1:1 marked the onset of water−water domains which resulted in the N−H group in $Ehim^+$ experiencing stronger hydrogen bonds.

The data presented here demonstrate that in the absence of water, $EhimNTf_2$ and $EmimNTf_2$ are significantly different. Atomistic simulations demonstrated that the $Ehim^+$ and $Emim^+$ cations experience different anionic interactions based on hydrogen bonding strength. The stronger interactions between cations and anions result in $EhimNTf_2$ having a higher viscosity. At low water content, water has little impact on the chemical environment of the $Ehim^+$ cation. However, at the 1:1 concentration, the liquid structure of $EhimNTf_2$ fundamentally changes due to preferential water−water interactions changing the cationic environment. This is in contrast to $EmimNTf_2$, which has limited water interactions at all water concentrations.

AUTHOR INFORMATION

Corresponding Author

*Phone: 650 723-4446; E-mail: fayer@stanford.edu.

ORCID

Yong-Lei Wang: 0000-0003-3393-7257

Michael D. Fayer: 0000-0002-0021-1815

Notes

The authors declare no competing financial interest.

ACKNOWLEDGMENTS

We thank Patrick L. Kramer, Joseph E. Thomaz, and Steven A. Yamada for helpful discussions and Chiara H. Giammanco for experimental assistance. Patrick L. Kramer also assisted in the deuteration of $EhimNTf_2$. The experimental work was funded by Division of Chemistry, Directorate of Mathematical and Physical Sciences, National Science Foundation (NSF) (CHE-1461477). In addition, Y.-L. Wang gratefully acknowledges the financial support from Knut and Alice Wallenberg Foundation (KAW 2015.0417). Quantum chemistry *ab initio* calculations and atomistic molecular dynamics simulations were performed using computational resources provided by Swedish National Infrastructure for Computing (SNIC) at HPC2N and NSC, and computational resources on the Sherlock cluster at Stanford University.

REFERENCES

(1) Castner, E. W.; Margulis, C. J.; Maroncelli, M.; Wishart, J. F. Ionic Liquids: Structure and Photochemical Reactions. *Annu. Rev. Phys. Chem.* **2011**, *62*, 85−105.

(2) Hayes, R.; Warr, G. G.; Atkin, R. Structure and Nanostructure in Ionic Liquids. *Chem. Rev.* **2015**, *115*, 6357−6426.

(3) Greaves, T. L.; Drummond, C. J. Protic Ionic Liquids: Evolving Structure−Property Relationships and Expanding Applications. *Chem. Rev.* **2015**, *115*, 11379−11448.

(4) Greaves, T. L.; Drummond, C. J. Protic Ionic Liquids: Properties and Applications. *Chem. Rev.* **2008**, *108*, 206−237.

(5) Dong, K.; Zhang, S. Hydrogen Bonds: A Structural Insight into Ionic Liquids. *Chem. - Eur. J.* **2012**, *18*, 2748−2761.

(6) Angell, C. A.; Byrne, N.; Belieres, J.-P. Parallel Developments in Aprotic and Protic Ionic Liquids: Physical Chemistry and Applications. *Acc. Chem. Res.* **2007**, *40*, 1228−1236.

(7) MacFarlane, D. R.; Tachikawa, N.; Forsyth, M.; Pringle, J. M.; Howlett, P. C.; Elliott, G. D.; Davis, J. H.; Watanabe, M.; Simon, P.; Angell, C. A. Energy Applications of Ionic Liquids. *Energy Environ. Sci.* **2014**, *7*, 232−250.

(8) Summers, C. A.; Flowers, R. A. Protein Renaturation by the Liquid Organic Salt Ethylammonium Nitrate. *Protein Sci.* **2000**, *9*, 2001−2008.

DOI: 10.1021/acs.jpcb.7b06376
J. Phys. Chem. B XXXX, XXX, XXX−XXX

(9) Gurkan, B. E.; de la Fuente, J. C.; Mindrup, E. M.; Ficke, L. E.; Goodrich, B. F.; Price, E. A.; Schneider, W. F.; Brennecke, J. F. Equimolar CO_2 Absorption by Anion-Functionalized Ionic Liquids. *J. Am. Chem. Soc.* **2010**, *132*, 2116−2117.
(10) Heldebrant, D. J.; Yonker, C. R.; Jessop, P. G.; Phan, L. Reversible Uptake of COS, CS_2, and SO_2: Ionic Liquids with O-Alkylxanthate, O-Alkylthiocarbonyl, and O-Alkylsulfite Anions. *Chem. - Eur. J.* **2009**, *15*, 7619−7627.
(11) Lewandowski, A.; Świderska-Mocek, A. Ionic Liquids as Electrolytes for Li-ion Batteries—An Overview of Electrochemical Studies. *J. Power Sources* **2009**, *194*, 601−609.
(12) Menne, S.; Vogl, T.; Balducci, A. Lithium Coordination in Protic Ionic Liquids. *Phys. Chem. Chem. Phys.* **2014**, *16*, 5485−5489.
(13) Yasuda, T.; Watanabe, M. Protic Ionic Liquids: Fuel Cell Applications. *MRS Bull.* **2013**, *38*, 560−566.
(14) Widegren, J. A.; Laesecke, A.; Magee, J. W. The Effect of Dissolved Water on the Viscosities of Hydrophobic Room-Temperature Ionic Liquids. *Chem. Commun.* **2005**, 1610−1612.
(15) Seddon, K. R.; Stark, A.; Torres, M.-J. Influence of Chloride, Water, and Organic Solvents on the Physical Properties of Ionic Liquids. *Pure Appl. Chem.* **2000**, *72*, 2275.
(16) Blanchard, J. W.; Belieres, J.-P.; Alam, T. M.; Yarger, J. L.; Holland, G. P. NMR Determination of the Diffusion Mechanisms in Triethylamine-Based Protic Ionic Liquids. *J. Phys. Chem. Lett.* **2011**, *2*, 1077−1081.
(17) Varela, L.; Carrete, J.; Turmine, M.; Rilo, E.; Cabeza, O. Pseudolattice Theory of the Surface Tension of Ionic Liquid− Water Mixtures. *J. Phys. Chem. B* **2009**, *113*, 12500−12505.
(18) Anouti, M.; Jacquemin, J.; Lemordant, D. Transport Properties of Protic Ionic Liquids, Pure and in Aqueous Solutions: Effects of the Anion and Cation Structure. *Fluid Phase Equilib.* **2010**, *297*, 13−22.
(19) Yaghini, N.; Nordstierna, L.; Martinelli, A. Effect of Water on the Transport Properties of Protic and Aprotic Imidazolium Ionic Liquids−An Analysis of Self-Diffusivity, Conductivity, and Proton Exchange Mechanism. *Phys. Chem. Chem. Phys.* **2014**, *16*, 9266−9275.
(20) Mele, A.; Tran, C. D.; De Paoli Lacerda, S. H. The Structure of a Room-Temperature Ionic Liquid with and without Trace Amounts of Water: The Role of C- H··· O and C- H··· F Interactions in 1-n-Butyl-3-Methylimidazolium Tetrafluoroborate. *Angew. Chem.* **2003**, *115*, 4500−4502.
(21) Driver, G.; Huang, Y.; Laaksonen, A.; Sparrman, T.; Wang, Y.-L.; Westlund, P.-O. Correlated/Non-Correlated Ion Dynamics of Charge-Neutral Ion Couples: The Origin of Ionicity in Ionic Liquids. *Phys. Chem. Chem. Phys.* **2017**, *19*, 4975−4988.
(22) Sturlaugson, A. L.; Arima, A. Y.; Bailey, H. E.; Fayer, M. D. Orientational Dynamics in a Lyotropic Room Temperature Ionic Liquid. *J. Phys. Chem. B* **2013**, *117*, 14775−14784.
(23) Sturlaugson, A. L.; Fruchey, K. S.; Fayer, M. D. Orientational Dynamics of Room Temperature Ionic Liquid/Water Mixtures: Evidence for Water-Induced Structure and Anisotropic Cation Solvation. *J. Phys. Chem. B* **2012**, *116*, 1777−1787.
(24) Bhargava, B.; Yasaka, Y.; Klein, M. L. Computational Studies of Room Temperature Ionic Liquid−Water Mixtures. *Chem. Commun.* **2011**, *47*, 6228−6241.
(25) Méndez-Morales, T.; Carrete, J. s.; Cabeza, O.; Gallego, L. J.; Varela, L. M. Molecular Dynamics Simulation of the Structure and Dynamics of Water−1-Alkyl-3-methylimidazolium Ionic Liquid Mixtures. *J. Phys. Chem. B* **2011**, *115*, 6995−7008.
(26) Wang, Y.-L.; Sarman, S.; Kloo, L.; Antzutkin, O. N.; Glavatskih, S.; Laaksonen, A. Solvation Structures of Water in Trihexyltetradecylphosphonium-orthoborate Ionic Liquids. *J. Chem. Phys.* **2016**, *145*, 064507.
(27) Wang, Y.-L.; Shimpi, M. R.; Sarman, S.; Antzutkin, O. N.; Glavatskih, S.; Kloo, L.; Laaksonen, A. Atomistic Insight into Tetraalkylphosphonium Bis(oxalato)borate Ionic Liquid/Water Mixtures. 2. Volumetric and Dynamic Properties. *J. Phys. Chem. B* **2016**, *120*, 7446−7455.
(28) Turton, D. A.; Sonnleitner, T.; Ortner, A.; Walther, M.; Hefter, G.; Seddon, K. R.; Stana, S.; Plechkova, N. V.; Buchner, R.; Wynne, K. Structure and Dynamics in Protic Ionic Liquids: A Combined Optical Kerr-Effect and Dielectric Relaxation Spectroscopy Study. *Faraday Discuss.* **2012**, *154*, 145−153.
(29) Hunger, J.; Sonnleitner, T.; Liu, L.; Buchner, R.; Bonn, M.; Bakker, H. J. Hydrogen-Bond Dynamics in a Protic Ionic Liquid: Evidence of Large-Angle Jumps. *J. Phys. Chem. Lett.* **2012**, *3*, 3034−3038.
(30) Krüger, M.; Bründermann, E.; Funkner, S.; Weingärtner, H.; Havenith, M. Communications: Polarity Fluctuations of the Protic Ionic Liquid Ethylammonium Nitrate in the Terahertz Regime. *J. Chem. Phys.* **2010**, *132*, 101101.
(31) Mamontov, E.; Luo, H.; Dai, S. Proton Dynamics in N, N, N′, N′-tetramethylguanidinium Bis (perfluoroethylsulfonyl) imide Protic Ionic Liquid Probed by Quasielastic Neutron Scattering. *J. Phys. Chem. B* **2009**, *113*, 159−169.
(32) Docampo-Álvarez, B.; Gómez-González, V.; Méndez-Morales, T.; Carrete, J.; Rodríguez, J. R.; Cabeza, Ó.; Gallego, L. J.; Varela, L. M. Mixtures of Protic Ionic Liquids and Molecular Cosolvents: A Molecular Dynamics Simulation. *J. Chem. Phys.* **2014**, *140*, 214502.
(33) Chang, T.-M.; Dang, L. X.; Devanathan, R.; Dupuis, M. Structure and Dynamics of N, N-diethyl-N-methylammonium Triflate Ionic Liquid, Neat and with Water, from Molecular Dynamics Simulations. *J. Phys. Chem. A* **2010**, *114*, 12764−12774.
(34) Wang, Y.-L.; Lyubartsev, A.; Lu, Z.-Y.; Laaksonen, A. Multiscale Coarse-Grained Simulations of Ionic Liquids: Comparison of Three Approaches to Derive Effective Potentials. *Phys. Chem. Chem. Phys.* **2013**, *15*, 7701−7712.
(35) Urahata, S. M.; Ribeiro, M. C. Structure of Ionic Liquids of 1-Alkyl-3-methylimidazolium Cations: A Systematic Computer Simulation Study. *J. Chem. Phys.* **2004**, *120*, 1855−1863.
(36) Giraud, G.; Gordon, C. M.; Dunkin, I. R.; Wynne, K. The Effects of Anion and Cation Substitution on the Ultrafast Solvent Dynamics of Ionic Liquids: A Time-Resolved Optical Kerr-Effect Spectroscopic Study. *J. Chem. Phys.* **2003**, *119*, 464−477.
(37) Kinoshita, S.; Sakai, Y.; Miyazaki, J.; Watanabe, J. Fundamental Aspects of Light Scattering and Optical Kerr Effect Spectroscopy. *Eur. Phys. J.: Spec. Top.* **2012**, *209*, 1−100.
(38) Smith, N. A.; Meech, S. R. Optically-Heterodyne-Detected Optical Kerr Effect (OHD-OKE): Applications in Condensed Phase Dynamics. *Int. Rev. Phys. Chem.* **2002**, *21*, 75−100.
(39) Li, J.; Cang, H.; Andersen, H. C.; Fayer, M. A Mode Coupling Theory Description of the Short-and Long-Time Dynamics of Nematogens in the Isotropic Phase. *J. Chem. Phys.* **2006**, *124*, 014902.
(40) Götze, W.; Sjögren, L. The Mode Coupling Theory of Structural Relaxations. *Transp. Theory Stat. Phys.* **1995**, *24*, 801−853.
(41) Nicolau, B. G.; Sturlaugson, A.; Fruchey, K.; Ribeiro, M. C. C.; Fayer, M. D. Room Temperature Ionic Liquid-Lithium Salt Mixtures: Optical Kerr Effect Dynamical Measurements. *J. Phys. Chem. B* **2010**, *114*, 8350−8356.
(42) Sturlaugson, A. L.; Fruchey, K. S.; Lynch, S. R.; Aragon, S. R.; Fayer, M. D. Orientational and Translational Dynamics of Polyether/Water Solutions. *J. Phys. Chem. B* **2010**, *114*, 5350−5358.
(43) Sokolowsky, K. P.; Bailey, H. E.; Fayer, M. D. Length Scales and Structural Dynamics in Nematogen Pseudonematic Domains Measured with 2D IR Vibrational Echoes and Optical Kerr Effect Experiments. *J. Phys. Chem. B* **2014**, *118*, 7856−7868.
(44) Sokolowsky, K. P.; Bailey, H. E.; Fayer, M. D. New Divergent Dynamics in the Isotropic to Nematic Phase Transition of Liquid Crystals Measured with 2D IR Vibrational Echo Spectroscopy. *J. Chem. Phys.* **2014**, *141*, 194502.
(45) Frisch, M. J.; Trucks, G. W.; Schlegel, H. B.; Scuseria, G. E.; Robb, M. A.; Cheeseman, J. R.; Scalmani, G.; Barone, V.; Petersson, G. A.; Nakatsuji, H.; et al. *Gaussian 09*; Gaussian Inc.:Wallingford, CT, 2009.
(46) Becke, A. D. Density-Functional Exchange-Energy Approximation with Correct Asymptotic Behavior. *Phys. Rev. A: At., Mol., Opt. Phys.* **1988**, *38*, 3098.

DOI: 10.1021/acs.jpcb.7b06376
J. Phys. Chem. B XXXX, XXX, XXX−XXX

(47) Lee, C.; Yang, W.; Parr, R. G. Development of the Colle-Salvetti Correlation-Energy Formula into a Functional of the Electron Density. *Phys. Rev. B: Condens. Matter Mater. Phys.* **1988**, *37*, 785.
(48) Breneman, C. M.; Wiberg, K. B. Determining Atom-Centered Monopoles from Molecular Electrostatic Potentials. The Need for High Sampling Density in Formamide Conformational Analysis. *J. Comput. Chem.* **1990**, *11*, 361−373.
(49) Wang, Y.-L.; Shah, F. U.; Glavatskih, S.; Antzutkin, O. N.; Laaksonen, A. Atomistic Insight into Orthoborate-Based Ionic Liquids: Force Field Development and Evaluation. *J. Phys. Chem. B* **2014**, *118*, 8711−8723.
(50) Liu, Z.; Huang, S.; Wang, W. A Refined Force Field for Molecular Simulation of Imidazolium-Based Ionic Liquids. *J. Phys. Chem. B* **2004**, *108*, 12978−12989.
(51) Hess, B.; Kutzner, C.; Van Der Spoel, D.; Lindahl, E. GROMACS 4: Algorithms for Highly Efficient, Load-Balanced, and Scalable Molecular Simulation. *J. Chem. Theory Comput.* **2008**, *4*, 435−447.
(52) Palese, S.; Schilling, L.; Miller, R. D.; Staver, P. R.; Lotshaw, W. T. Femtosecond Optical Kerr Effect Studies of Water. *J. Phys. Chem.* **1994**, *98*, 6308−6316.
(53) Taschin, A.; Bartolini, P.; Eramo, R.; Righini, R.; Torre, R. Optical Kerr Effect of Liquid and Supercooled Water: The Experimental and Data Analysis Perspective. *J. Chem. Phys.* **2014**, *141*, 084507.
(54) Torre, R.; Bartolini, P.; Righini, R. Structural Relaxation in Supercooled Water by Time-Resolved Spectroscopy. *Nature* **2004**, *428*, 296−299.
(55) Annapureddy, H. V.; Hu, Z.; Xia, J.; Margulis, C. J. How Does Water Affect the Dynamics of the Room-Temperature Ionic Liquid 1-Hexyl-3-methylimidazolium Hexafluorophosphate and the Fluorescence Spectroscopy of Coumarin-153 When Dissolved in it? *J. Phys. Chem. B* **2008**, *112*, 1770−1776.
(56) Perrin, F. Mouvement Brownien d'un Ellipsoide-I. Dispersion Diélectrique Pour des Molécules Ellipsoidales. *J. Phys. Radium* **1934**, *5*, 497−511.
(57) Dote, J. L.; Kivelson, D.; Schwartz, R. N. A Molecular Quasi-Hydrodynamic Free-Space Model for Molecular Rotational Relaxation in Liquids. *J. Phys. Chem.* **1981**, *85*, 2169−2180.
(58) Allison, S. A. Low Reynolds Number Transport Properties of Axisymmetric Particles Employing Stick and Slip Boundary Conditions. *Macromolecules* **1999**, *32*, 5304−5312.
(59) Hu, C.-M.; Zwanzig, R. Rotational Friction Coefficients for Spheroids with the Slipping Boundary Condition. *J. Chem. Phys.* **1974**, *60*, 4354−4357.
(60) Tirado, M. M.; de la Torre, J. G. Rotational Dynamics of Rigid, Symmetric Top Macromolecules. Application to Circular Cylinders. *J. Chem. Phys.* **1980**, *73*, 1986−1993.
(61) Youngren, G. K.; Acrivos, A. Rotational Friction Coefficients for Ellipsoids and Chemical Molecules with the Slip Boundary Condition. *J. Chem. Phys.* **1975**, *63*, 3846−3849.
(62) Sension, R. J.; Hochstrasser, R. M. Comment On: Rotational Friction Coefficients for Ellipsoids and Chemical Molecules with Slip Boundary Conditions. *J. Chem. Phys.* **1993**, *98*, 2490−2490.
(63) Bondi, A. van der Waals Volumes and Radii. *J. Phys. Chem.* **1964**, *68*, 441−451.
(64) Abe, H.; Takekiyo, T.; Shigemi, M.; Yoshimura, Y.; Tsuge, S.; Hanasaki, T.; Ohishi, K.; Takata, S.; Suzuki, J.-i. Direct Evidence of Confined Water in Room-Temperature Ionic Liquids by Complementary Use of Small-Angle X-ray and Neutron Scattering. *J. Phys. Chem. Lett.* **2014**, *5*, 1175−1180.
(65) Wong, D. B.; Sokolowsky, K. P.; El-Barghouthi, M. I.; Fenn, E. E.; Giammanco, C. H.; Sturlaugson, A. L.; Fayer, M. D. Water Dynamics in Water/DMSO Binary Mixtures. *J. Phys. Chem. B* **2012**, *116*, 5479−5490.
(66) Martinelli, A. Conformational Changes and Phase Behaviour in the Protic Ionic Liquid 1-Ethylimidazolium Bis (trifluoromethylsulfonyl) imide in the Bulk and Nano-Confined State. *Eur. J. Inorg. Chem.* **2015**, *2015*, 1300−1308.
(67) Wong, D. B.; Giammanco, C. H.; Fenn, E. E.; Fayer, M. D. Dynamics of Isolated Water Molecules in a Sea of Ions in a Room Temperature Ionic Liquid. *J. Phys. Chem. B* **2013**, *117*, 623−635.
(68) Moilanen, D. E.; Fenn, E. E.; Wong, D.; Fayer, M. D. Water Dynamics in Large and Small Reverse Micelles: From Two Ensembles to Collective Behavior. *J. Chem. Phys.* **2009**, *131*, 014704.
(69) Kramer, P. L.; Giammanco, C. H.; Fayer, M. D. Dynamics of water, methanol, and ethanol in a room temperature ionic liquid. *J. Chem. Phys.* **2015**, *142*, 212408.
(70) Giammanco, C. H.; Kramer, P. L.; Wong, D. B.; Fayer, M. D. Water Dynamics in 1-Alkyl-3-Methylimidazolium Tetrafluoroborate Ionic Liquids. *J. Phys. Chem. B* **2016**, *120*, 11523−11538.

DOI: 10.1021/acs.jpcb.7b06376
J. Phys. Chem. B XXXX, XXX, XXX−XXX